INSTITUTE OF PHYSICS PUBLISHING JOURNAL OF PHYSICS: CONDENSED MATTER

J. Phys.: Condens. Matter **18** (2006) S2713–S2736 doi:10.1088/0953-8984/18/38/S13

Nanostructures and ordering phenomena in ferrofluids investigated using polarized small angle neutron scattering

A Wiedenmann, M Kammel, A Heinemann and U Keiderling

Hahn-Meitner Institut Berlin GmbH, Glienickerstraße 100 D-14109 Berlin, Germany

E-mail: Wiedenmann@hmi.de

Received 2 May 2006, in final form 24 July 2006
Published 8 September 2006
Online at stacks.iop.org/JPhysCM/18/S2713

Abstract

Polarized small angle neutron scattering (SANSPOL) was used to investigate the microstructure of various ferrofluids (FF) where magnetic materials (Co, Fe magnetite), stabilization mechanisms (electrostatic, monolayers and bilayers of surfactants) and carrier liquids (water, organic solvents) have been systematically varied. Magnetic core–shell particles, non-magnetic micelles and magnetic aggregates were identified and size distributions and density, composition, and magnetization profiles were determined. Partial penetrations of solvent molecules inside the surfactant layer and formation of non-magnetic oxide coatings were established. The magnetic nanostructure in diluted samples consists of non-interacting ferromagnetic single domain particles. In concentrated Co FF a pseudo-crystalline ordering was found to be induced by an external magnetic field where cobalt core–shell particles are arranged in hexagonal planes. The particle ordering and magnetic moment direction followed the direction of the applied field. In addition, segments of uncorrelated dipolar chains were found to be present. The dynamics of the field induced ordering was studied by means of time-resolved SANS. Individual particle moments are stuck by field induced dipolar interactions in domains of local hexagonal ordering which relax by rotational diffusion when the field is switched off, with a characteristic time of a few seconds.

(Some figures in this article are in colour only in the electronic version)

1. Introduction

Magnetic colloids are stable dispersions of ferromagnetic materials. In such 'ferrofluids' (denoted as FF) nanoscaled magnetic particles are stabilized against coagulation either by electrostatic repulsion or by coating the core with organic chain molecules acting as surfactants. Synthesis, characterization, rheological and magnetic properties as well as applications have

been recently reviewed in [1–3]. Various applications are based on the superparamagnetic behaviour of single domain nanosized particles. In fact, if screening of the surfactants is inefficient the particles might grow to larger sizes and form multidomain ferromagnetic structures. Therefore a precise knowledge of the microstructural parameters is a prerequisite for the interpretation of macroscopic phenomena and for a tailored fabrication of FF. Small angle neutron scattering (SANS) is perfectly adapted to study the mesoscopic constituents of FF. The advantages of neutrons are obvious: (i) samples can be investigated *in situ* in the liquid state, (ii) the strong scattering power of hydrogen contained in the organic surfactants gives access to the shell, and (iii) the interaction of the neutron spin with magnetic moments allows one to visualize the magnetism of the core. However, complications arise in polydisperse systems when different constituents are present. Then we face the problem that weak magnetic scattering signals have to be analysed beside strong nuclear contributions from other sources or vice versa, which can lead to considerable inconsistencies in the interpretation of results. In our SANS investigations we used polarized neutrons as a labelling technique for the magnetic part. Combined with the isotope contrast variation, the parameters of size, distribution and composition of the particles as well as magnetic nanostructures have been determined systematically depending on the magnetic materials, surfactants and carrier liquids and on the particle concentration.

The paper is organized as follows. In section 2 we recall the basic concept of SANS when polarized neutrons are used. Details of preparation and the experimental set-up for SANS are given in section 3. Characteristics of nanostructural constituents as obtained from diluted samples of various ferrofluids will be presented in section 4.1. Section 4.2 focuses on the inter-particle correlations which are relevant for concentrated ferrofluids when a magnetic field is applied. The nature of field induced local ordering in various concentrated systems has been studied as a function of strength and orientation of the magnetic field. In section 4.3 a dynamical study of the magnetization reversal by a new technique of time dependent stroboscopic SANS is presented. Some common features are discussed in section 4.4. Finally, a summary is given in section 5.

2. The technique of small angle neutron scattering

Small angle neutron scattering (SANS) is a non-destructive technique for analysing density, concentration and magnetization fluctuations on a nanometre length scale [4, 5]. Elastic scattering of neutrons of wavelength λ around the primary beam occurs at an angle 2Θ which corresponds to the scattering vector Q of magnitude $Q = |\boldsymbol{Q}| = 4\pi \sin\Theta/\lambda$. The scattered intensity $I(\boldsymbol{Q})$ is the square of the total amplitude and measured in reciprocal space. By Fourier transform of $I(\boldsymbol{Q})$ the correlation functions are obtained in real space giving access to size, composition and magnetization of inhomogeneities present in the material. In polydisperse multiphase systems different types of particles j of different shapes $f_j(QR)$ and size distributions $N_j(R)$ coexist. All inhomogeneities contribute to the SANS scattering signal and might superimpose within the same Q range when the different particles are of similar sizes. The scattering intensity is then given [6, 7] by monodisperse subsystems weighted by the size distributions according to

$$I(Q) = \sum_{j=1}^{N} \int_0^\infty N_j F_j^2(QR) N_j(R) S_j(Q)\, \mathrm{d}R. \tag{1}$$

$F(QR) = \int \mathrm{d}r^3 \Delta\eta \exp(\mathrm{i}\boldsymbol{Q}\boldsymbol{r}) = \Delta\eta V_\mathrm{p} f(QR)$ is the total amplitude or form factor obtained by summing up the scattering amplitudes of all atoms weighted by the phase shift at each

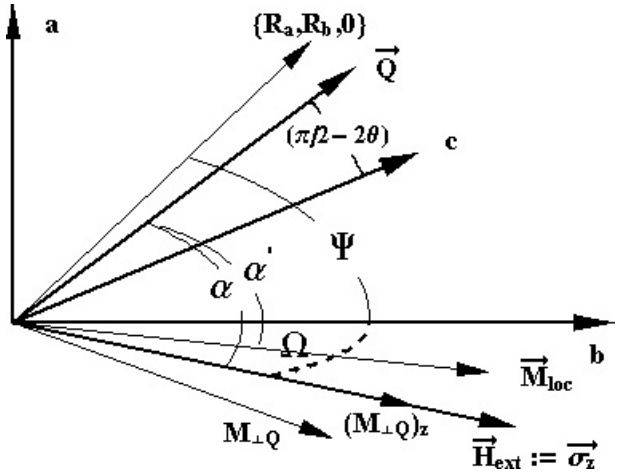

Figure 1. Definitions of the external magnetic field H_{ext}, local magnetization M_{loc} scattering vector Q with respect to the orthogonal detector coordinates ab and incoming neutron beam c.

atomic position $\boldsymbol{r}$. The contrast $\Delta\eta$ is the difference between scattering length densities of particle and matrix, i.e. $\Delta\eta = \eta_{\text{p}} - \eta_{\text{matrix}}$ which can be nuclear or magnetic. For nuclear scattering $\eta_{\text{N}} = \Sigma c_i b_i/\Omega_i$, where b_i is the nuclear scattering length, c_i the concentration and Ω_i the atomic volume of the species i. In the magnetic scattering length density $\boldsymbol{\eta}_M = (e^2\gamma/2mc^2)\Sigma c_i M_i^{\perp}/\Omega_i$, only the projection of the magnetic moment $M_i^{\perp}$ onto a plane perpendicular to the scattering vector $\boldsymbol{Q}$ contributes to the interaction. The shape factor $f(QR)$ is known analytically for various simple geometrical units. The scattered intensity depends on the form factors $F_j(\boldsymbol{QR})$ and partial structure factors $S_j(\boldsymbol{Q})$ of all particles. When particles are fully uncorrelated the structure factors $S_j(Q)$ in equation (1) will be unity as in the case of a perfect gas or in disordered condensed matter where the scattering at large values of Q is determined mainly by the form factor of the particles alone.

For *polarized neutrons* the neutron spins are defined by the external magnetic field $\boldsymbol{H}_{\text{ext}}(\boldsymbol{z} \parallel \boldsymbol{H})$ and denoted by $(+)$ when aligned antiparallel, or parallel $(-)$ to a preferred orientation $\boldsymbol{z}$. If the polarization of the scattered neutrons is not analysed one can distinguish between $I(\boldsymbol{Q}, -)$ and $I(\boldsymbol{Q}, +)$ scattering by switching a spin flipper in front of the sample on and off, respectively. This technique, denoted as SANSPOL was described in detail in [8–10]. Let P ($\approx$1) denote the degree of polarization for $(+)$ neutrons and ε the spin-flipper efficiency ($\varepsilon \approx 1$) when activated and $\varepsilon = 0$ for flipper 'off'. For diluted systems where $S(Q) = 1$ (see e.g. [11]) the intensities for the two polarization states $I(\boldsymbol{Q}, \pm)$ evaluate to:

$$I(\boldsymbol{Q}, \pm) = F_{\text{N}}(\boldsymbol{Q})^2 + \boldsymbol{F}_{\text{M}}^{\perp}(\boldsymbol{Q})\boldsymbol{F}_{\text{M}}^{\perp}(\boldsymbol{Q}) + 4P(\varepsilon - 1/2)F_{\text{N}}(\boldsymbol{Q})\boldsymbol{F}_{\text{M}}^{\perp}(\boldsymbol{Q})_z. \tag{2}$$

$F_{\text{N}}(Q)$ is the nuclear form factor and $\boldsymbol{F}_{\text{M}}^{\perp}(\boldsymbol{Q})_z$ is the z-component of the magnetic scattering amplitude where z is defined by the direction of the external field $\boldsymbol{H}_{\text{ext}}$. $I(\boldsymbol{Q}, -)$ is obtained from equation (2) for $\varepsilon(-) = 1$ while for $I(\boldsymbol{Q}, +)\varepsilon(+) = 0$.

Generally, only the magnetization perpendicular to $\boldsymbol{Q}$ contributes to the magnetic scattering. Using the definitions in figure 1 the intensity difference (or cross-term) reads

$$I(\boldsymbol{Q}, -) - I(\boldsymbol{Q}, +) = 4P F_N(\boldsymbol{Q})\boldsymbol{F}_{\text{M}}^{\perp}(\boldsymbol{Q})(\cos\angle(\boldsymbol{M}_{\text{loc}}, \boldsymbol{H}_{\text{ext}}) - \cos\alpha\cos\alpha'), \tag{3}$$

where only the component in the external field direction contributes to the scattering. For pure magnetic contributions $\boldsymbol{F}_{\text{M}}^{\perp}(\boldsymbol{Q})\boldsymbol{F}_{\text{M}}^{\perp}(\boldsymbol{Q})$ has a simple $\sin^2\alpha$ dependence. In the special

case where $\boldsymbol{M}_{\rm loc}$ is aligned along $\boldsymbol{H}_{\rm ext}$ ($\cos\angle(\boldsymbol{M}_{\rm loc}, \boldsymbol{H}_{\rm ext}) = 1$ and $\alpha = \alpha'$) equation (3) is simplified to

$$I(\boldsymbol{Q}, -) - I(\boldsymbol{Q}, +) = 4PF_{\rm N}(\boldsymbol{Q})F_{\rm M}(\boldsymbol{Q})\sin^2\alpha, \tag{4}$$

which shows the same dependence on the angle α as the pure magnetic term. In the data analysis one has to distinguish between these angles and the angle Ψ between the position vector of a detector cell counting a scattered neutron at $\{R_a, R_b, 0\}$ and the b-axes in the natural orthogonal a–b–c system spanned by the 2D detector and the incoming neutron beam c. Even in experiments were $\boldsymbol{H}$ is aligned parallel to the b-axis the difference is fundamental for the scattering of anisotropic structures like orientated chains. The $\boldsymbol{Q}$-vector in the a–b–c system is given by

$$\boldsymbol{Q} = Q\{\cos\Theta\cos\Psi, \cos\Theta\sin\Psi, -\sin\Theta\} \tag{5}$$

showing always a (small) component out of the detector plane in the direction of the incoming neutron beam. In particular, if the $\boldsymbol{H}$ and/or $\boldsymbol{M}$ fields are out of the a–b plane, even for isotropic scattering like core–shell particles the full $\boldsymbol{Q}$-vector is required for data interpretation.

The intensities $I(\boldsymbol{Q}, +)$ and $I(\boldsymbol{Q}, -)$ are different for the two polarization states for any angle α except for $\alpha = 0$. When the direction of $\boldsymbol{M}_{\rm loc}$ is not exactly parallel to $\boldsymbol{H}$, the difference $I(\boldsymbol{Q}, +) - I(\boldsymbol{Q}, -)$ is no longer zero for $\boldsymbol{Q}$ parallel to the $\boldsymbol{H}$ direction. The remaining terms in equation (2) are identical for scattering of non-polarized neutrons and affected only by the angle α' between $\boldsymbol{M}_{\rm loc}$ and $\boldsymbol{Q}$. Since the SANSPOL intensity difference is linear in nuclear and magnetic form factors it allows the sign and magnitude of the nuclear with respect to magnetic contributions to be evaluated with great precision. It will be essential for 2D data analysis where the orientation between $\boldsymbol{H}$ and the 2D detector can be changed during the experiment. As a direct consequence we can detect deviations of the local magnetization direction from that of the external field only in the cross-term, that means by the use of polarized neutrons.

In the case of *non-perfect alignment* of the magnetic moments of a ferromagnetic single domain particle of saturation magnetization $M_{\rm s}^{\rm p}$ embedded in a non-magnetic matrix [10, 12, 13] superparamagnetic behaviour is expected. Then the orientation distribution of the magnetic moments as a function of an effective magnetic field $H_{\rm eff}$ and temperature follows the Langevin statistics $L(x) = \coth(x) - 1/x$, where the argument is given by $x = M(R)H_{\rm eff}/k_{\rm B}T$. The total magnetic moment, $M(R)$, depends on the radius R of the particles according to $M(R) = 4\pi R^3 m_0/3\Omega$, where m_0 is the atomic magnetic moment and Ω is the atomic volume, respectively. The two different SANSPOL intensities $I(-)(Q, \alpha)$ and $I(+)(Q, \alpha)$ are given by (assuming $P = 1$)

$$\begin{aligned} I(-, +)(\boldsymbol{Q}, \alpha) = \{&[F_{\rm M}^2 L^2(x) \pm 2F_{\rm M}F_{\rm N}L(x)]\sin^2\alpha + F_{\rm N}^2\}S(\boldsymbol{Q}, \alpha) \\ &+ F_{\rm M}^2\{2L(x)/x - \sin^2\alpha[L^2(x) - 1 + 3L(x)/x)]\}, \end{aligned} \tag{6}$$

where steric interaction effects were taken into account via phenomenological structure factors $S(\boldsymbol{Q}, \alpha)$. The first term in equation (6) is a contribution which is affected by nuclear and/or magnetic inter-particle correlations defined by $S(Q, \alpha)$, while the second term results solely from non-perfect alignment of the magnetic moments of individual particles [14]. This last term vanishes when the magnetic particle moment is perfectly aligned along $\boldsymbol{H}$ where, for $x \to \infty$ $L(x)/x = 0$.

The intensity difference between the two polarization states given by

$$I(-)(\boldsymbol{Q}, \alpha) - I(+)(\boldsymbol{Q}, \alpha) = 4F_{\rm N}F_{\rm M}L(x)S(\boldsymbol{Q}, \alpha)\sin^2\alpha. \tag{7}$$

The average of $[I(-) + I(+)(\boldsymbol{Q}, \alpha)]/2$ corresponds to the intensity of non-polarized SANS.

3. Experimental details

3.1. Sample preparation

Magnetite nanoparticles (Fe_3O_4) can be produced by a simple and reproducible wet chemical procedure [15, 16]. By mixing solutions of $FeCl_2$ and $FeCl_3$ in ammonium magnetite nanoparticles are precipitated:

$$2FeCl_3 + FeCl_2 + 8NH_3 + 4H_2O \rightarrow Fe_3O_4 + 8NH_4Cl.$$

Both temperature and reaction time have an influence on the size distribution of the nanoparticles. All investigated magnetite nanoparticles of the series ELEC, DEX, LM1 have been produced by this method by the Berlin Heart AG company. A second type of magnetite nanoparticles has been obtained from bacteria. The ability of magnetotactic bacteria to orient and migrate along geomagnetic field lines is based on intra-cellular magnetic structures, the magnetosomes. In most cases they consist of nanometre sized crystals of the magnetite covered by a protein and lipid membrane. Bacteria, magnetospirillum gryphiswaldense, were grown micro-aerobically [17]. The magnetosomes were isolated and purified by centrifugation and subsequently treated in a magnetic separation column. This was performed by the Max Planck Institute for Marine Microbiology, Bremen. Iron particles were synthesized by thermal decomposition of iron pentacarbonyl $Fe(CO)_5$ in decalin under the presence of oleic acid [18]. All samples were kept under nitrogen atmosphere in order to prevent oxidation of the particles. These samples of the series OA3 were prepared by K Butter of the University of Utrecht. Cobalt nanoparticles of all investigated Co ferrofluids (series MFT, MA) have been produced in a two step process by thermolysis of $Co_2(CO)_8$ according to [19, 20]:

$$2Co_2(CO)_8 \leftrightarrow Co_4(CO)_{12} + 4CO; \qquad Co_4(CO)_{12} \leftrightarrow 4Co + 12CO.$$

The series MFT has been prepared by Berlin Heart AG in different isotope mixtures of toluene and in technical oil 'L9' as carrier liquid. A second series (MA) was produced by Max Planck Institute für Kohlenforschung, Mühlheim. A narrow size distribution of Co particles is obtained when the thermolysis is produced under the presence of aluminium alkyls (all MA series) [21]. By varying the alkyl chain length and the ratio of cobalt to aluminium the particle size can be adjusted between 3 and 15 nm. Air stable suspensions were prepared by introducing a stream of synthetic dry air into the ferrofluid sample (series MA77, MA85, MA95).

Stable magnetic colloids have been obtained by three different kinds of protection of the nanoparticles against aggregation (see table 1). After precipitation in the wet chemical procedure magnetite nanoparticles remain with a surface charge. Electrostatic repulsion of these charges protects the magnetite nanoparticles against agglomeration [22]. Sample ELEC was prepared in such a way. A second stabilization technique utilized dextran to cover the magnetite particles. The molecular chains of dextran were entangled by subsequent heat treatments (series DEX). Magnetic nanoparticles stabilized with different surfactants have been investigated in the series OLE1, LM1, MFT, MA and OA3. Different types of surfactants can be used for the stabilization of the same nanoparticles in a broad range of particle concentration. The series OLE1 and MA-44 were prepared with oleoylsarkosine (OLE) $C_{17}H_{33}$–CO–NCH_3–CH_2–COOH, LM1 with a mixture of a dodecanoic acid $C_{11}H_{23}COOH$ and C_{12} ethoxylated alcohol $CH_2(CH_3)_{11}$–O–$(CH_2$–$CH_2O)_9$–H, for MFT MA77, MA85 and MA95 with a mixture based on oleoylsarkosine as the main compound and two other surfactants. (Hyp9100 and PIBSI). Different solvents including water, toluene, technical oil 'L9' and others have been used. In some cases the solvents have been deuterated for a contrast variation and for reducing the incoherent neutron scattering background.

Table 1. List of samples investigated by SANS and main parameters as obtained by the present SANS investigations: $\langle R_c \rangle$: average core radius, D_{sh}: shell thickness, $\langle R_A \rangle$ and $\langle R_{Mic} \rangle$: average radii of aggregates and non-magnetic micelles, respectively.

Label [ref]	Prepared by	Magn. nano-particle	Stabilization	Solvent	$\langle R_c \rangle$ (nm)	D_{shell} (nm)	$\langle R_A \rangle$ (nm)	$\langle R_{Mic} \rangle$ (nm)
ELEC	Berlin Heart AG	Fe_3O_4	Electrostatic	$H_{0.2}D_{1.8}O$	4	—	9.8	—
DEX	Berlin Heart AG	Fe_3O_4	Dextran coated	$H_{0.2}D_{1.8}O$	4.8	2.4	16.8	—
LM1	Berlin Heart AG	Fe_3O_4	Surfactants: do-decanoic acid/ C_{12} ethoxylated alcohol	$H_{0.2}D_{1.8}O$ $H_{0.4}D_{1.6}O$ H_1D_1O	6.7 6.7 6.7	2.7 2.7 2.7	17.8 22.8 12.3	2.6 2.6 2.6
OLE1-Wat	Berlin Heart AG	Fe_3O_4	Surfactant: oleoylsarkosine	$H_{0.84}D_{1.16}O$ $H_{0.54}D_{1.46}O$	5.0 5.0	2.3 2.3	14.2 16.2	2.3 2.3
OLE1-Tol	Berlin Heart AG	Fe_3O_4	Surfactant: oleoylsarkosine	$C_7H_{3.2}D_{4.8}$ C_7 $H_{1.36}D_{6.64}$	5.0 5.0	1.9 1.9	13.6 16.3	1.4 1.4
Magneto-some Type A Type B	MPI Bremen	Fe_3O_4	Protein and lipid membrane	 D_2O D_2O	 15.6 21.8	 4.0 3.4		
MFT DS1–DS5	Berlin Heart AG	Co	Surfactant: oleoylsarkosine and other	Toluene	3.7	1.9	—	1.8
MFT3	Berlin Heart AG	Co	Surfactants: oleoylsarkosine and other	'L9'	4.4	1.9	—	1.8
MA44	MPI Mühl-heim	Co	Surfactant: oleoylsarkosine	C_7D_8	2.9	1.9		
MA77/ MA85	MPI Mühl-heim	Co	Surfactants: oleoylsarkosine and other	$C_7H_4D_4$ C_7H_8	4.6 3.8	**1.4** /1.3 **1.5** ***CoO***		1.8
MA95	MPI Mühl-heim	Co	Surfactants: oleoylsarkosine and other	Toluene H8	4.4	1.9	—	—
OA3	Univ. Utrecht	$Fe_{0.75}C_{0.25}$	Oleic acid	Decalin	3.4	2.0		

3.2. SANS experiment

SANS measurements have been performed at the instrument V4 installed at the BERII reactor of HMI, Berlin [23]. Magnetic fields up to 1.1 T were applied perpendicular and up to 6 T parallel to the incoming neutron beam, respectively. In the conventional mode non-polarized neutrons of $\lambda = 0.6$ nm with $\Delta\lambda/\lambda = 0.11$ have been used. Polarized neutrons were provided by a transmission polarizing supermirror cavity [24]. The two scattering intensities $I(+)$ and $I(-)$ were cumulated alternatively with flipper off and on. The SANSPOL option, which can be set without any modification of the instrument alignment, is characterized by a high neutron flux of more than 30% of non-polarized neutrons, a high degree of polarization ($P = 95\%$) and by the high efficiency of the spin flipper ($\varepsilon(-) \approx 98\%$). The accessible Q range of 0.08–3 nm^{-1} allowed particles of radii from 0.5 to 80 nm to be detected. The scattering

intensities collected in the 2D detector of 128 × 128 cells with a pixel size of 0.25 cm^2 were corrected cell by cell for background, efficiencies and transmissions and calibrated on absolute scale (in cm^{-1} sr^{-1}) using the data reduction package BERSANS [25]. One dimensional data of $I(+)(Q,\alpha)$, $I(-)(Q,\alpha)$, the averages $0.5[I(+)(Q,\alpha) + I(-)(Q,\alpha)]$ and differences $[I(-)(Q,\alpha) - I(+)(Q,\alpha)]$ were obtained by regrouping the 2D data in angle sectors of 10° widths at various angles α between $\boldsymbol{H}$ and $\boldsymbol{Q}$. These 1D data have been analysed with model fitting programs (e.g. FISH, SASFiT, Mathematika) using least squares routines where the actual values of P and f are taken into account. When several SANSPOL or SANS curves were used simultaneously, constraints between the model parameters could be introduced in the fits [26].

4. Results

4.1. Nanostructured constituents of ferrofluids

Structural properties such as size, distributions, composition and magnetic moments of different constituents of FF have been determined in very diluted samples where inter-particle correlations can be neglected, i.e. where structure factor $S(Q) = 1$ in equation (6) can be assumed. Microstructural changes have been elucidated by a variation of the core material, stabilizing surfactant and carrier liquids [27]. From these studies it turned out that stable samples cannot be prepared in a free choice of the microstructural parameters but some of the parameters are interdependent, e.g. increasing the concentration of magnetic particles in Co FF was only possible when large excess of surfactants are added.

4.1.1. Nuclear and magnetic nanostructures of Co FF. SANSPOL measurements have been performed on cobalt ferrofluid samples (MA44) [26, 28]. With non-polarized neutrons magnetic and nuclear intensities are obtained separately as the squared form factors weighted by the corresponding size distributions. This may give rise to serious ambiguities when in polydispersed multiphase systems magnetic and non-magnetic objects of similar size are present. In contrast for SANSPOL the cross-term of equation (7) occurs only between nuclear and magnetic amplitude from one and the same particle. This behaviour enabled us to distinguish between 'composite' particles built up by a magnetized core of Co atoms surrounded by a non-magnetic surface layer from non-magnetic particles of similar size. Such a 'composite' can be described by a shell model consisting of a sphere with an inner core radius R' surrounded by a concentric shell of radius R. The form factor is given by

$$F_{c\text{-shell}}(Q) = [(\Delta\eta_1 - \Delta\eta_2) f_{\text{sph}}(QR') + \Delta\eta_2 f_{\text{sph}}(Q(R))]V_{\text{p}} \tag{8}$$

with the shape function for spheres $f_{\text{sph}}(x) = 3[\sin(x) - x\cos(x)]/x^3$.

For SANSPOL the scattering contrasts with respect to the matrix are different for the magnetic core and non-magnetic shell and given by $\Delta\eta_1^{(-,+)} = \eta_1^{\text{nuc}} \pm \eta_1^{\text{mag}} - \eta_{\text{matrix}}$ and $\Delta\eta_2 = \eta_2^{\text{nuc}} - \eta_{\text{matrix}}$, respectively. In the present case, only $\Delta\eta_1^{(\pm)}$ depends on the polarization. For non-polarized neutrons the nuclear and magnetic contrasts for the core are given by $\Delta\eta_1^{(\text{nuc})} = \eta_1^{\text{nuc}} - \eta_{\text{matrix}}^{\text{nuc}}$ and by $\Delta\eta_1^{(\text{mag})} = \eta_1^{\text{mag}}$, respectively, while for the shell $\Delta\eta_2^{\text{nuc}} = \eta_2^{\text{nuc}} - \eta_{\text{matrix}}$ and $\Delta\eta_2^{(\text{mag})} = 0$.

The SANSPOL intensity difference (equation (7)) results only from magnetic particles while all separate non-magnetic contributions are cancelled out. This feature makes the difference very sensitive to density and magnetization profiles. In the present case a set of the parameters precisely fit the SANSPOL difference shown in figure 2, lhs. However, these parameters cannot explain the full scattering curves $I(-)$ and $I(+)$, respectively, as

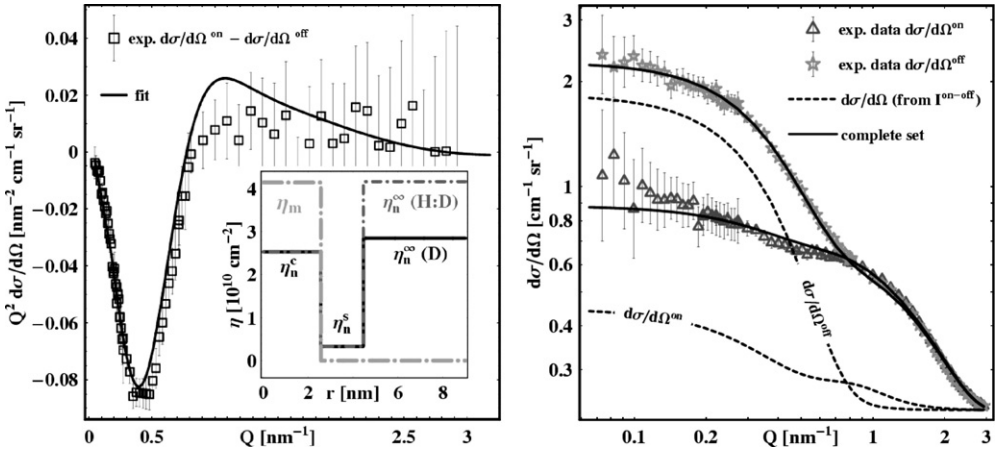

Figure 2. SANSPOL scattering curves of Co FF MA44 for $\alpha = 90°$ [28]. lhs: experimental SANSPOL difference $(I(\text{on}) - I(\text{off}))Q^2$ (squares) and least squares fit (solid line) using the scattering length density profile as shown in the inset for different solvents. rhs: $I(\text{on})$ and $I(\text{off})$. Dashed lines: Contributions of magnetic particles as obtained from a fit to the SANSPOL difference (lhs). Solid lines: simultaneous fit including non-magnetic contributions from micelles.

demonstrated by the dashed lines in figure 2, rhs. Obviously, an additional non-magnetic constituent has to be taken into account. This non-magnetic contribution results from the excess of surfactants used in the preparation and which may form micelles of similar size. Figure 2, rhs, shows the results of a simultaneous least squares fit of the SANSPOL intensities $I(+)(Q \perp H)$ and $(I-)(Q \perp H)$ and the SANS intensities $F_N(Q)^2$ and $F_M(Q)^2$ using the form factor of core–shell particles. All data were fitted with analytical gamma particle size distributions for the core–shell particles and micelles. For the smaller non-magnetic particles a mean radius of $R_s = 1.1$ nm, a variance of $\sigma_s = 0.2$ nm, and a scattering length density for oleoylsarkosine is obtained. The core–shell particles have a mean radius of $\langle R_c \rangle = 2.9$ nm and a variance of $\sigma_c = 0.8$ nm. The thickness of the shell $D = 1.9$ nm for the non-magnetic layer and $\eta_{sn} = 0.5 \times 10^{10}$ cm^{-2} for the shell indicate that this layer also consists of oleoylsarkosine. The magnetic scattering length of the core corresponds to the bulk value of cobalt.

4.1.2. Oxide coating of Co ferrofluids. In order to study the origin of the considerable stability of the Co FF on exposure to air samples from different preparations have been investigated and compared. Two samples were prepared with the step of smooth oxidation namely MA85 and MA77 in toluene. The sample MA44 was prepared in toluene without smooth oxidation. The solvent of MA85 was not deuterated, while in MA44 deuterated and MA77 partly deuterated toluene has been used. The SANSPOL data have been analysed with a constrained fitting procedure using a model which included a magnetic core and one or two non-magnetic shells corresponding to a possible oxide layer covered by the usual shell of surfactants [29]. In figure 3 the SANSPOL curves $I(-)(Q \perp H)$ and $I(+)(Q \perp H)$ (symbols) are compared for both samples. For the MA85 the intensity of $I(+)$ revealed a maximum at $Q = 0.75$ nm^{-1} while $I(-)$ increases continuously. This is characteristic for core–shell structures. Since the solvent in this sample was not deuterated there is no scattering contrast between the surfactant material and the solvent. Nevertheless the constrained fit (lines in figure 3) with a core–shell model gave a good agreement with the observed scattering cross-sections. The mean radius of the core was found to be 3.84 ± 0.03 nm with a variance of 0.75 ± 0.02 nm. The magnetic and

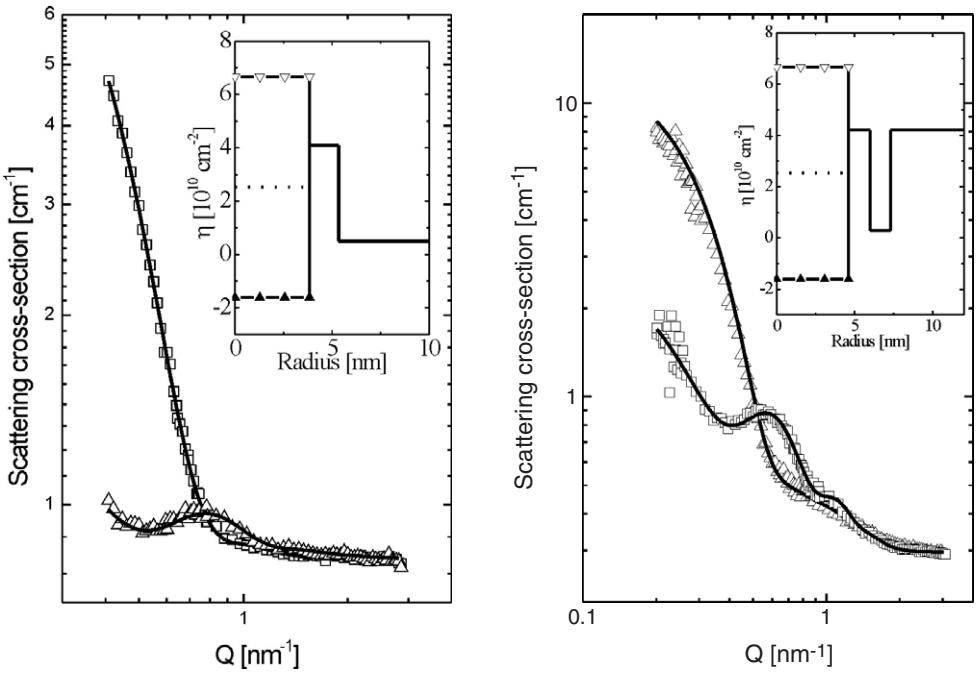

Figure 3. Experimental data and fitted scattering cross-sections $I(+)$ (triangles) and $I(-)$ (squares) of the MA85 (lhs), MA77 (rhs) cobalt ferrofluids. The lines are the results of a constrained fit of a core–shell model shown in the insets [29].

nuclear scattering length densities of the magnetic Co core were fixed to the theoretical values of cobalt. The shell was found to be non-magnetic with a thickness of $D = 1.5 \pm 0.1$ nm with a fitted scattering length density of the shell $\eta_S = (4.1 \pm 0.5) \times 10^{10}$ cm^{-2}. This value is higher than that for cobalt ($\eta = 2.53 \times 10^{10}$ cm^{-2}) and differs strongly from that of the surfactant Koranthin SH ($\eta = 0.33 \times 10^{10}$ cm^{-2}). It is however very close to the theoretical scattering length density of CoO with $\eta = 4.41 \times 10^{10}$ cm^{-2}. We therefore conclude that this layer produced by the smoothed oxidation consist of non-magnetic CoO.

When deuterated solvents were used the high scattering contrast of the surfactant leads to more complicated scattering patterns. In the case of smoothed oxidation two different kinds of shells should be manifested in deuterated samples, one of the Co oxide layer and a second one of the surfactant shell. Figure 3 shows the scattering cross-sections of the partly deuterated samples MA77. Effectively, the whole data set (lines in figure 3) could only be fitted when an additional second non-magnetic shell was assumed. The thickness of the first layer was found to be 1.4 ± 0.5 nm with a scattering length density of $(4.2 \pm 0.2) \times 10^{10}$ cm^{-2}. These parameters are in good agreement with the results of the sample MA85. The scattering length density of the second layer with a thickness of 1.3 ± 0.3 nm was fixed to the theoretical value of Koranthin SH. The magnetic core showed a mean radius of 4.6 ± 0.3 nm and a variance of 0.6 ± 0.1 nm. As shown in section 4.1.1 a second fraction of non-magnetic particles with a mean radius of 1.8 ± 0.6 nm, had to be taken into account which are ascribed to micelles of free surfactant material [27]. For the sample MA44 prepared without the step of smooth oxidation a model with a magnetic core, a non-magnetic shell and a second fraction of non-magnetic particles is sufficient to fit the data (see section 4.1.1). There was no evidence for a cobalt oxide layer. In summary, SANSPOL showed clearly that all Co samples prepared with

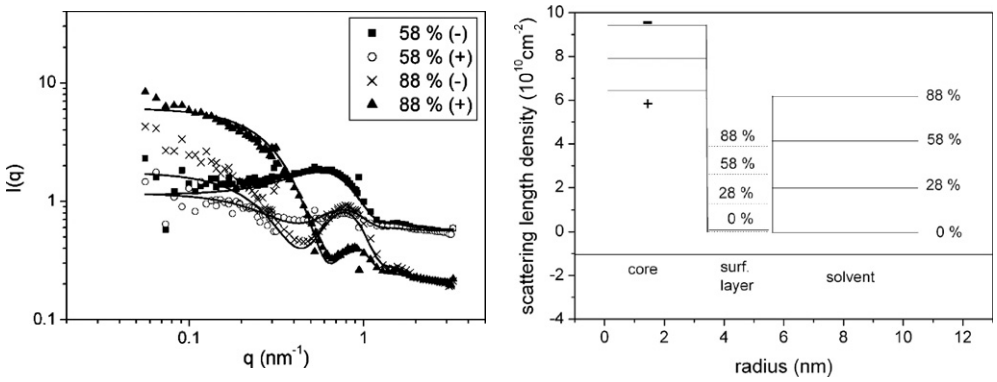

Figure 4. lhs: SANSPOL scattering curves of $Fe_{0.7}C_{0.25}$ ferrofluids for different volume fractions of deuterated decalin. The solid curves are fits according to a core–shell model with partial penetration of solvent in the surfactant shell with the scattering length density profiles of the rhs [30].

the smooth oxidation show a layer of CoO which apparently protects the nanosized Co core from further oxidation.

4.1.3. Iron ferrofluids. SANSPOL investigations of iron nanoparticles [30] with different isotope mixtures of the solvent are presented in figure 4, lhs. All $I(+)$ and $I(-)$ curves could be fitted fairly well with a core–shell model with log-normal distribution of the core radius. The resulting scattering length density (figure 4, rhs) of the core corresponds to the composition $Fe_{0.75}C_{0.25}$. Inside the shell η_{sh} was found to depend on the isotope compositions of the solvent which must be ascribed to a partial penetration of the solvent into the oleic acid shell. The amount of solvent inside the oleic acid layer was found to be 62%. The evolution of the nanostructure of the ferrofluids was followed when samples were exposed to air. The SANSPOL curves of these oxidized particles could be well fitted with a two shell model consisting of the magnetic core surrounded by a non-magnetic Fe oxide layer and the shell of surfactants.

4.1.4. Investigations of the stabilization mechanism. Three different types of stabilization mechanisms have been analysed in magnetite based ferrofluids: (i) particles covered by a dextran layer, (ii) coated by a surfactant layer (LM1), and (iii) electrostatically stabilizes particles [31, 32]. Isotope contrast variation has been used in samples prepared with different H/D ratios in the solvent. From a SANSPOL study [31] it turned out that in the DEX sample the magnetite cores $\langle R_c \rangle = 4.8$ nm are covered by a non-magnetic surface layer. No surface layer was found in the ELEC sample where $\langle R_c \rangle$ of the spherical nanocrystals of magnetite is 4.0 nm. However, a second fraction of magnetite particles with a average radius 2–3 times larger than the core were detected resulting from aggregation due to imperfect screening. In addition to these particles in the LM1 sample a third fraction of non-magnetic particles was found consisting of surfactant material [32]. The resulting scattering length density of the shell was found to be independent of the H/D composition of the solvent, which indicates that the organic surfactant is nearly impenetrable for the solvent.

4.1.5. Solvent dependent bonding of surfactants. Magnetite nanoparticles coated with oleoylsarkosine (denoted as OLE) can be stabilized in water as well as in toluene as solvents. The open question concerned the bonding of OLE to the magnetic particle which could be

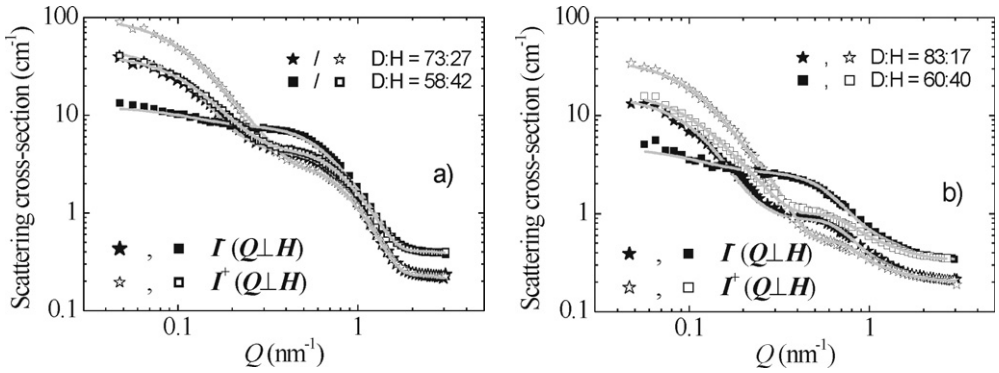

Figure 5. SANSPOL curves of magnetite ferrofluids OLE1-Wat (a) and OLE1-Tol (b). The different H/D ratios of the carrier liquids are indicated in the figures. The scattering cross-sections are given by filled symbols for neutron spin parallel to H, $I(-, Q \perp H)$, and by open symbols for neutron spin antiparallel to H, $I(+, Q \perp H)$). The solid lines represent the fits with the derived structural model of core–shell particles, aggregates and free excess surfactants.

mediated by the central electron pair of nitrogen or via the hydrophilic acid group. There are two possibilities for the binding mechanism in case of polar and non-polar solvents: if oleoylsarkosine couples with the nitrogen atom on the magnetite particle surface, then the hydrophilic acid group of oleoylsarkosine is available for the solubility in polar solvents. In this case a monolayer of surfactants should built up. If the surfactant couples via the hydrophilic acid group, a bilayer is necessary for the solubility in polar solvents. In non-polar solvents the surfactant always forms a monolayer that is sufficient for solubility.

The different types of bonding between particle and shell should be reflected in the thickness of the surfactant layer in the two different solvents. A precise determination of the shell thickness was necessary in order to answer the question of the binding mechanism [33]. Magnetite particles dispersed in water (OLE1-Wat) as a polar solvent and in toluene as a non-polar solvent (OLE1-Tol) have been studied with different H/D ratios of the carrier liquid. In figure 5 the SANSPOL scattering curves $I(-, Q \perp H)$ and $I(+, Q \perp H)$ are shown. The differences between the two polarization states measured at one and the same H/D ratio indicates the presence of magnetic nanostructures. The combined chemical and magnetic contrast variation gave sufficient information (figure 5), which allowed all structural parameters of the model to be fitted consistently. Three structural parts were analysed by a simultaneous fit of all four scattering curves. Besides the core–shell particles and aggregates, non-magnetic free surfactant structures were identified in both the water and toluene based ferrofluids.

The averaged sizes and the volume fractions of all three components of the four samples are summarized in table 1. It turned out that the shell thicknesses clearly depend on the solvents: in a non-polar solvent the layer thickness of (1.9 ± 0.1 nm) is effectively characteristic for a monolayer just as found in other cobalt ferrofluids. However, in a polar solvent the shell is significantly larger which must correspond to a bilayer where the hydrophobic chains interpenetrate leading to an observed thickness of 2.3 ± 0.1 nm. These results indicate that bonding of the surfactants to the magnetic core is mediated via the hydrophilic acid group and not via the nitrogen atom. The aggregates have nearly the same size distributions in both solvents but they are always slightly larger and contain less magnetite in the sample with higher deuteration. These results are ascribed to the fact that the aggregates are mixtures of magnetite and shell molecules. Dilution with the deuterated solvents also leads to a decrease of magnetization and magnetic contrast of the aggregates.

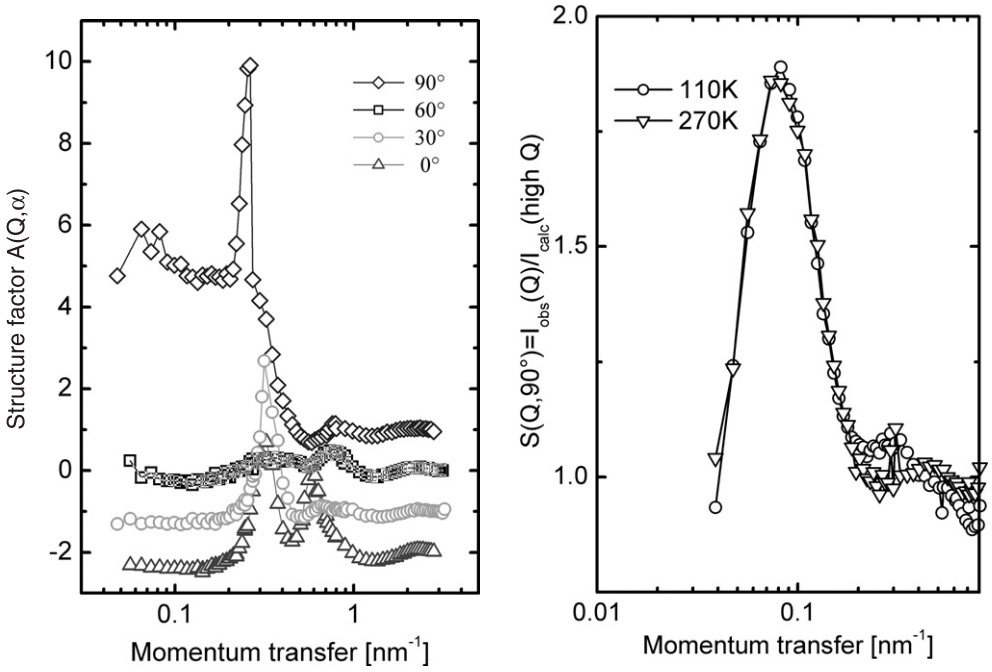

Figure 6. Anisotropic effective structure factors for 3 vol% Co FF [34]. lhs: in-plane correlations at angles α. The ordinates at $\alpha = 60°$, 30° and 0°, were shifted by -1, -2 and -3 units with respect to that of 90°. rhs: out-of-plane structure factors at two temperatures.

4.2. Particle correlations induced by magnetic fields

4.2.1. Nature of inter-particle correlations. Inter-particle correlation under the influence of an external magnetic field has been studied on the series of Co FF samples (MFT DS1–DS6) with different Co concentrations from 0.2 to 6 vol% but with exactly the same particle size distribution [34]. When a magnetic field of 1 T was applied *perpendicular* to the incoming beam in all samples with Co concentrations above 1 vol% pronounced anisotropic correlation peaks occur in the 2D patterns which are indexed with the Miller indices as shown in figure 7. Six peaks appear at Q_1 forming angles of $\alpha = \pm 30°, \alpha = \pm 90°$ and $\pm 150°$, two peaks at $Q_2 = \sqrt{3} * Q1$ at $\alpha = 0°$ and 180° and two additional peaks at Q_3 at $\alpha = \pm 90°$, respectively. All peaks disappeared in zero field. The total structure factors $S(Q, \alpha)$ for a given orientation α have been derived by dividing the measured SANSPOL intensities $I \pm (Q, \alpha)$ at a given sector angle α by those measured in very diluted samples. Whenever the latter was not available we used instead the intensities calculated by using the particle data $(R_0, D, N(R), \sigma, \eta)$ as obtained from the fit of the intensities at high Q-values, where $S(Q, \alpha) = 1$ was assumed [34]. Apart from the sector at $\alpha = 0°$ it was more convenient to use the difference pattern $I(-) - I(+)$ for the evaluation of $S(Q, \alpha)$. When the magnetic field was applied *parallel* to the incoming neutrons a diffuse 'Debye–Scherrer' ring was observed at Q_3 corresponding to (001) reflections. The in-plane and out-of-plane structure factors are shown in figure 6. The positions of the observed correlation peaks correspond to a pseudo-crystalline ordering where the Co particles are arranged in hexagonal planes with the magnetic moments aligned along $\boldsymbol{H}$ as shown in figure 7. The arrangement of figure 7 is one of the fully equivalent textures which lead to the peaks at Q_3 when H is perpendicular to the incident

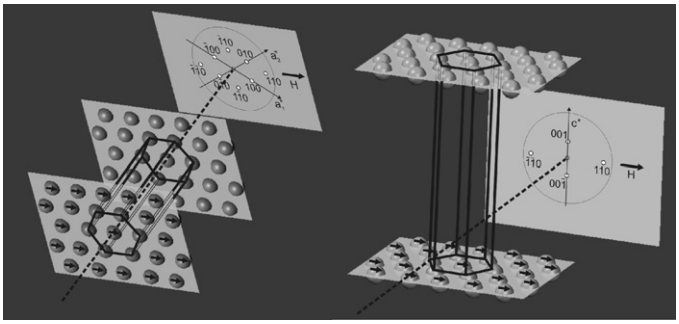

Figure 7. Schematic representation of particle arrangements in hexagonal symmetry in textures of type I (lhs) and type II (rhs) and the corresponding reciprocal lattice points observed in the detector plane. The horizontal magnetic field is perpendicular to the incident beam [34].

beam. Hexagonal layers are aligned along $\boldsymbol{H}$ but no preferred orientation of the locally ordered domains occurs perpendicular to $\boldsymbol{H}$. While the in-plane nearest neighbour distance was found to be almost independent of the concentration and temperatures the distance between neighbour planes c decreases with increasing concentration. The correlation length of the ordered domains induced by the external magnetic field was derived from the actual peak widths to about 120 nm, i.e. 4–5 'unit cells.'

For the diluted sample with 1 vol% Co no such peaks were observed in an external field. Instead, diffuse residual intensities occur in planes perpendicular to the magnetic field at $Q_x = 0$ and 0.29 nm^{-1} and much less pronounced at $Q_x = 0.58$ nm^{-1} which strongly indicates the presence of chain-like aggregates of particles. The magnetic dipoles are arranged in the (attractive) head to tail configuration and which are aligned along the magnetic field. Spontaneous chaining in zero field and coexistence of chains segments with hexagonal ordered domains has been observed when the magnetic field was increased [35].

4.2.2. Formation of partially ordered structures. The development of locally ordered structures has been investigated on a concentration series (0.5, 1, 2.5 and 5 vol%) of a cobalt based ferrofluid prepared by a new technique [21]. By using different magnetic fields (0.001–0.998 T) it is possible to influence solely the magnetic scattering contribution. From the most diluted ferrofluid we extracted the single particle information using a simultaneous regression analysis of this data with a convenient model. In order to evaluate possible ordering phenomena iso-intensity lines of the SANSPOL difference $(I(-) - I(+))/\sin^2\alpha$ are presented as a function of the angle α for different values of $|Q|$ [42]. In the case of an isotropic system we expect straight horizontal lines such as in the lhs of figure 8, where $F_N\ F_M$ was calculated using the parameter of the particles determined above. The fact that for a given Q-value the intensity depends only on $\sin^2\alpha$ reflects the isotropy of a random structure. Real experimental data are plotted for the diluted sample in the middle and at the bottom of figure 8 at $H = 0.003$ and 0.998 T, respectively, which are directly comparable to figure 8, top. Any deviation from horizontal iso-intensity lines must therefore result from anisotropic structure factor $S(Q, \alpha)$ such as at a high field of about 1 T: a very broad maximum appears at 90° which is interpreted as a scattering contribution from chaining of particles and orientated by the applied magnetic field (see [34, 35, 42]). For ferrofluids containing approximately 1 vol% of magnetic particles we observed the same structures but for 2.5 and 5 vol% new patterns appear. In figure 8, rhs, $I(Q, \alpha)$ pictures for three different fields are shown for 5 vol% sample. For the very weak magnetic fields of 0.003 T the pattern is dominated by the well-known form factor alone.

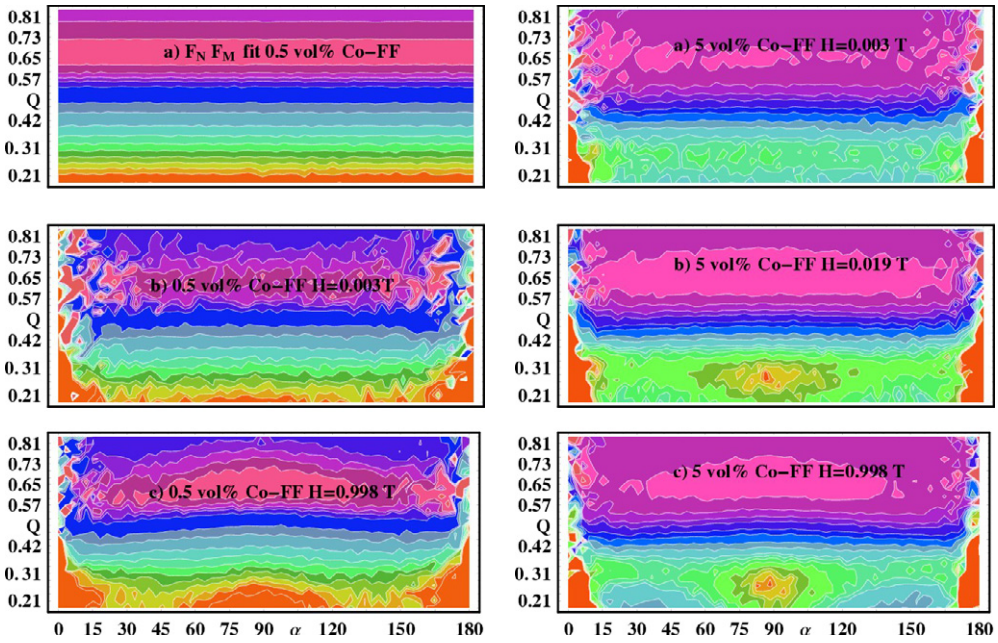

Figure 8. Iso-intensity plot of $(I(-) - I(+))/\sin^2\alpha$ as a function of the angle α. lhs: 0.5 vol% Co FF, top: calculated for $H = 0$, middle: observed at $H = 3$ mT and bottom: at $H = 0.998$ T. rhs: 5 vol% at different values of the applied magnetic field. After [42].

For slightly higher fields a new kind of peak structure appears. In figure 8 the change at 90° is the most obvious. At $Q = 0.29$ nm^{-1} a clearly separated peak occurs at 90° and discontinuities at 30° and 150° which are signatures for the previously observed hexagonal peaks. The resulting scattering patterns in a magnetic field are described as a convolution of single particle form factors, scattering from orientated chains and from pseudo-crystalline hexagonal structures see [34]. The contributions from each of this part depend on the particle sizes and size distribution, the concentration and the applied external field.

4.2.3. Field dependence of the ordering process

Variation of strength of the magnetic field. The field induced pseudo-crystalline ordering was confirmed in a second concentrated sample 'MFT3' with 6 vol% Co dispersed in oil L9 [35]. SANS revealed a highly uniform size of the Co particles with an average radius of 4.4 nm covered by a layer of surfactants with a thickness of about $D = 2$ nm. The position of the peaks at $Q_1 = 0.39$ nm^{-1} observed at $H = 1$ T, correspond to the hexagonal in-plane particle arrangement with a nearest neighbour distance $a(\text{hex}) = 4\pi/\sqrt{3}Q_1 = 18.9$ nm, while $Q_3 = 0.29$ nm^{-1} defines the stacking of the layers at a distance of $c(1\text{ T}) = 2\pi/Q_3 = 21.9$ nm. Both 'lattice constants' in MFT are shorter than in the DS samples despite the larger size of the particles in MFT, i.e. the overall packing density of the particles is higher in the case of the oil carrier. Peak positions and peak area were found to depend on the strength of the applied magnetic field. The variation of Q_3 corresponds to a strong decrease of the inter-plane distance from 27 nm at $H = 3$ mT to 21.9 nm at 1 T, respectively, while the in-plane nearest neighbour distance $a(\text{hex})$ changes only from 20 to 18.6 nm. This indicates that with increasing field an overall densification of the ordered domains occurs which is dominated

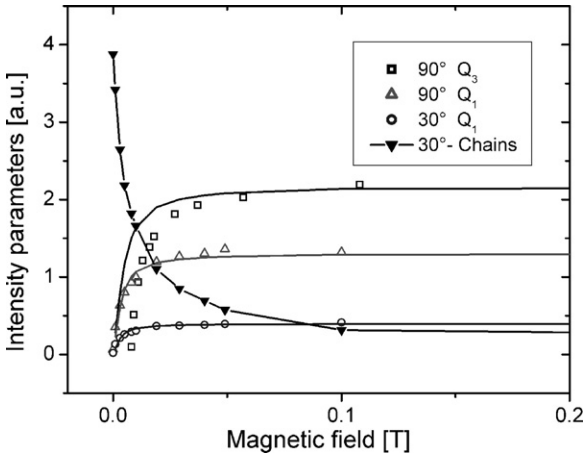

Figure 9. Field dependence of the scattering contributions from chain segments (solid triangles with line for guide to the eye at $\alpha = 30°$) and peak area at Q_1 and Q_3 (open symbols) with Langevin behaviour (solid line) [35].

by an increase of the correlations between neighbour layers. In zero magnetic field the two dimensional SANS pattern is perfectly isotropic. The isotropic average of the SANS intensities follow a Q^{-1} behaviour at low Q. This indicates that particle moments at zero field are spontaneously arranged in the attractive head to tail conformation in segments of uncorrelated chains. In fact, the low Q part of the zero field curve is well described by a random orientation of cylindrical objects with an average radius of 4.3 nm and length of about 27 nm, which corresponds to chain segments formed by about 3–4 particles [35, 36]. In strong fields these segments are aligned along $\boldsymbol{H}$ which leads to an increase of $S(Q, \alpha = 90°)$ and to diffuse residual intensities observed in planes perpendicular to the magnetic field at $Q_x = 0$ and $\pm 0.29\ \mathrm{nm}^{-1}$. A continuous transition from chain-like aggregates to layered structures has been detected in the MFT3 sample when the strength of $\boldsymbol{H}$ was increased. The SANSPOL difference patterns at $\alpha = 30°$ were analysed in terms of two contributions, $S_1(Q)$ corresponding to the pseudo-hexagonal ordering while $S_2(Q)$ is the contribution from cylindrical objects decaying at low Q with Q^{-1}. The field variation of the fitted parameters of the peaks at Q_1 and Q_3 (figure 9) showed that the segments are aligned along $\boldsymbol{H}$ already at very low values of $\boldsymbol{H}$ while the increase of the peaks follows the expected Langevin behaviour. When the field is increased instead of a continuous increase of the chain length segments are aggregated in layers forming more and more correlated pseudo-crystalline domains.

Variation of direction of the magnetic field. A horizontal cryomagnet was installed on a turntable to vary the angle between the incoming neutron and the external field $\boldsymbol{H}_{\mathrm{ext}}$ both spanning a plane perpendicular to the detector. By turning the cryomagnet ($\boldsymbol{\Omega}$-rotation; see figure 1) both the field and the sample change their orientations with respect to the neutron beam. Additionally the sample could be rotated independently ($\boldsymbol{\varphi}$-rotation). We performed three combinations of these rotational degrees of freedom and analysed the 2D scattering pattern with a newly developed fit procedure taking into account all influences of the varying orientation between $\boldsymbol{Q}$-vector and $\boldsymbol{H}_{\mathrm{ext}}$. Furthermore the use of polarized neutrons enables us to obtain also quantitative values for the form and structure factor parameters. Figure 10(d) shows the experimental 2D $I(\boldsymbol{Q}, +) - I(\boldsymbol{Q}, -)$ scattering pattern divided by the $\sin^2 \alpha$ ($\mathrm{d}\sigma/\mathrm{d}\Omega$ exp.)

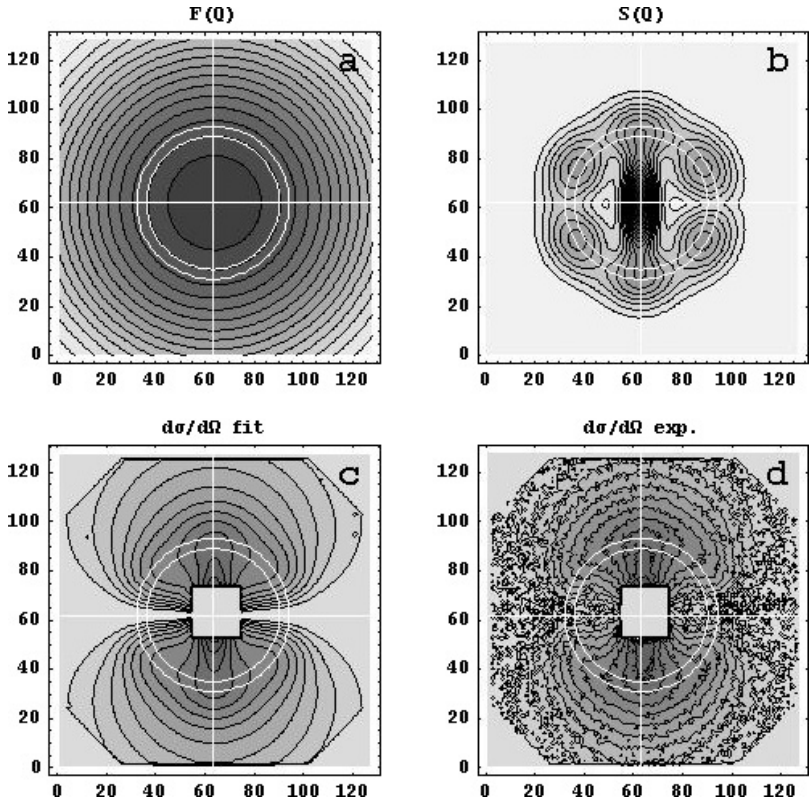

Figure 10. Cobalt based (MFT)FF. The experimental SANSPOL difference patterns $(I(-) - I(+))/\sin^2\alpha$ on a 2D detector (d) and results from a least squares fit for $\Omega = 0$ (c) using the particle form factor (a) and the structure factor (b).

and the fits for the (figure 10(c)) using the form factors (figure 10(a)) and structure factor figure 10(b)). In this configuration ($\Omega = 0, \varphi = 0$) the magnetic field is perpendicular to the neutron beam. The purely isotropic form factor $F(Q)$ is given by the properties of the single particles well known for this fluid by other, independent experiments. The structure factor $S(Q)$ was modelled using hexagonal peaks and the scattering from ellipsoids which simulates a possible arrangement to chain-like objects. In a least squares procedure, for all seven (Ω, φ) configurations we obtained the parameters of the peak position, peak height and the Gaussian widths. In order to discuss the influence of a field rotation we extracted the scattering intensity within the white ring as shown in figure 10, which contains the hexagonal peaks.

Figure 11 shows the result of this procedure for all (Ω, φ) configurations. The intensities are plotted versus the angle ψ between Q and the horizontal detector axes for different angles $\Omega = 0°, 10°, 20°, 30°, 40°, 50°$ and $60°$ (from bottom to top in figure 11). From figure 11 it is obvious, that by turning Ω the intensity of the hexagonal peaks decrease strongly. All curves have been fitted simultaneously with one parameter set namely $Q_1 = 0.39\ \mathrm{nm}^{-1}$ for the position of the peaks at $\alpha = \pm 30, \pm 90$ and ± 150 using the same values for the Gaussian widths of $\Delta Q = 0.09\ \mathrm{nm}^{-1}$ and $\Delta\alpha = 17°$ for all relative orientations of the magnetic field.

This result shows unambiguously that the magnetic moments are aligned along the external magnetic field. In addition, when the field was turned the particle moments had to rearrange in such a way that the local hexagonal ordering was conserved. From the width of the Gaussian

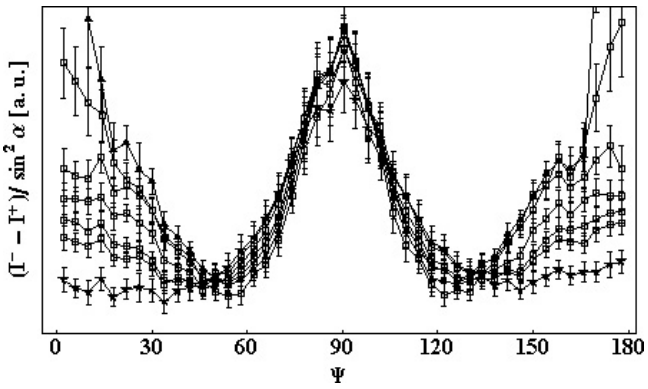

Figure 11. For the ring in the 2D detector (see figure 10(c)) at $Q = 0.39$ nm^{-1} the intensities $(I(Q,+) - I(Q,-))/\sin^2\alpha$ are plotted versus the angle ψ between Q and the horizontal detector axes. From bottom to top $\Omega = 0°$, 10°, 20°, 30°, 40°, 50° and 60°.

peaks the size of the ordered domains $\zeta = 2\pi/\Delta Q$ of about 70 nm is estimated, while $\Delta\alpha$ reflects a considerable orientational distribution.

4.2.4. Chain formation in magnetosomes. Two types of magnetosome suspensions (denoted as type A and B) have been cultivated under slightly different conditions. SANSPOL on samples highly diluted in D_2O revealed a rather sharp log-normal size distribution of the magnetite with a mean core radius of $\langle R_c \rangle = 21.8$ nm in sample B surrounded by a lipid shell of constant thickness of $D = 3.4$ nm while for the sample A $\langle R_c \rangle = 15.6$ nm and $D = 4$ nm [43]. The two dimensional SANS pattern for non-polarized neutrons of the higher concentrated type B sample is shown in figure 12, lhs. It is obvious that the iso-intensity lines are not of radial symmetry. Instead, we observe streaks of higher intensity in a vertical direction. The streak of the highest intensity goes through the centre at $Q_x = 0$ intermitted only by the beam stop (white rectangle). Two streaks occur to the left and to the right at $Q_{x1} = 0.1$ nm^{-1} and less pronounced at $Q_{x2} = 0.22$ nm^{-1}: such scattering pattern is characteristic for a one dimensional periodic arrangement of scattering objects, leading to equidistant planes perpendicular to the axis.

Apparently, the core–shell particles are arranged in chain-like structures that are aligned in the direction of the magnetic field. The projections of the scattering planes onto the detector then give rise to the observed streaks (dashed lines in figure 12, lhs). In order to evaluate quantitatively the anisotropic scattering, reciprocal lattice scans along the grey lines of figure 12, lhs, have been extracted by using azimuthal averaging in sectors of 15° width and plotted in figure 12, rhs. From the horizontal scan along the field direction (centred at $Q_y = 0$), the positions of the first and second order scattering planes are determined at $Q_{x1} = 0.11$ nm^{-1} and $Q_{x2} = 0.22$ nm^{-1}; respectively. This leads to the 'periodicity' $d = n2\pi/Q_{xn} = 57.1$ nm; which corresponds to the nearest neighbour distance of particle inside the chain. The other three scattering curves of figure 12, rhs, correspond to reciprocal lattice scans in vertical Q-directions perpendicular to the applied field and centred at $Q_x = 0$ (open circles) and $Q_{x1} = 0.11$ nm^{-1} (triangles). From the SANS behaviour at low Q, we conclude that particles are spontaneously arranged in short segments of chains, which in zero field are randomly distributed and get aligned along an applied magnetic field. Such chain segments have previously been observed in a TEM [17]. Comparing the d-value (57.1 nm) with the total particle size $2R = 50.4$ nm; we conclude that the lipid shells of neighbour particles nearly get in touch when they are arranged in chains. This is fully confirmed by a 2D model fitting of aligned cylindrical objects as shown in [44].

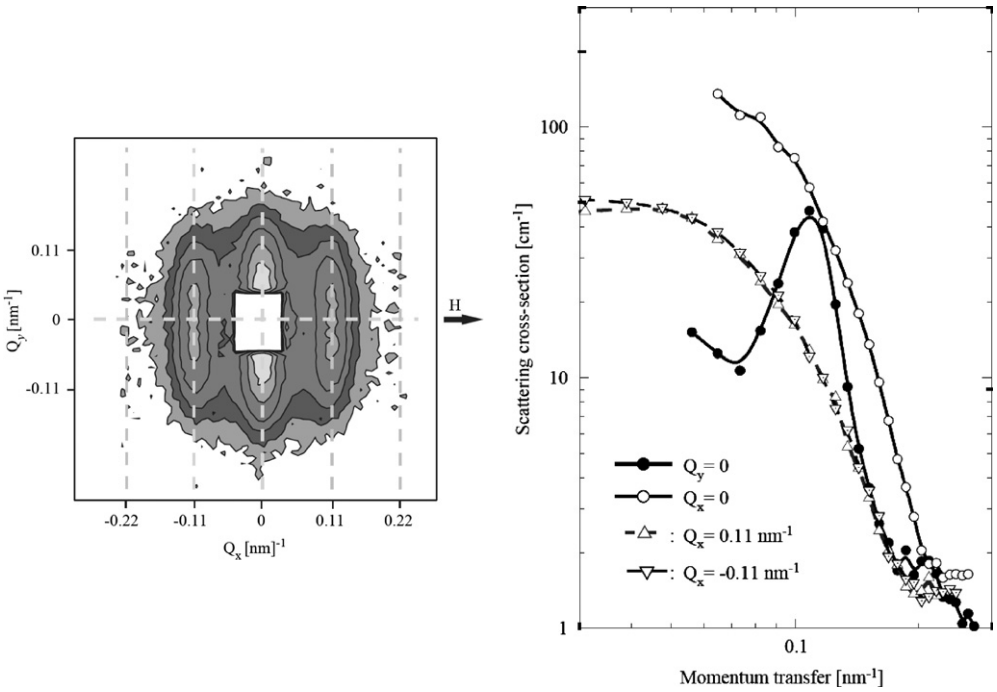

Figure 12. Lhs: 2D iso-intensity SANS pattern of a concentrated sample of type B in a horizontal magnetic field of 1 T and applied perpendicular to the incoming neutrons. The vertical dashed lines represent the quasi-1D scattering planes of zeroth, first and second order. rhs: reciprocal lattice scans calculated for azimuthally averaged sectors of 15° width and extracted along four grey lines in the figure lhs with centres at (0, 0) and (±0.11, 0), respectively.

4.3. Dynamics of relaxation of field induced ordering

A new time-resolved stroboscopic SANS technique has been set-up which allowed onset and decay of the local ordering to be measured with time constants of several 100 ms when the magnetic field is switched on and off. For details, see [37, 38]. SANSPOL scattering intensities $I(+)$ and $I(-)$ have been measured on the V4 instrument of HMI, Berlin and the D22 instrument at ILL, Grenoble, with incident neutron spin polarizations parallel $(-)$ and antiparallel $(+)$ to the magnetic field. The ferrofluid sample containing 6 vol% Co 'MFT3' [35] was placed in a homogeneous horizontal magnetic field H applied perpendicular to the incoming neutrons. At the D22 instrument the magnetic field could be switched off from 0.5 T to the remanence of 0.005 T within less than 100 ms. Time-frame histogram SANS measurements have been performed in time slices of 500 ms during a total time of 15 s after switching off the magnetic field. For raising and stabilization of the field at 0.5 T a waiting time of 5 s was intercalated. Sufficient counting statistics were obtained after 400–600 cycles. At the V4 SANS instrument the new readout system for the 2D detector is capable of producing list mode data which contain full discrete position and time information for each single neutron. For the present case of superparamagnetic single domain particles the sum signal $(I(+) + I(-))/2$ contains contributions from magnetic disorder of individual particle moments and from inter-particle correlations. In the SANSPOL difference intensity $I(-) - I(+)$ all disorder scattering is cancelled leaving the nuclear–magnetic interference term which results solely from magnetic particles and which contains an anisotropic structure factor $S(Q, \alpha)$ describing the inter-particle correlations.

As soon as the field is applied, ordering immediately sets in and is nearly completed long before the field reaches the maximum. The ordering occurs so quickly that the limiting factor for the measured ordering kinetics appears to be the slope of the field up-ramp, rather than the native dynamics of the sample structure. We therefore do not discuss the ordering process which needs different techniques to be applied [39]. The scattering patterns measured at $H = 0.5$ T and $H = 0$, respectively, turned out to be identical when measured in the stroboscopic cycling or in the static mode which demonstrated that the ordering–disordering process was really reversible. The 2D iso-intensity patterns have been averaged at angles $\alpha = 90°$ and 30° with respect to the horizontal direction of the magnetic field over a width of $\Delta\alpha = 20°$. The scattering intensities of the sum $(I(+) + I(-))/2$ and the difference intensities $I(-) - I(+)$ are shown in figure 13 as a function of the momentum transfer Q. Figure 13 reveals clearly the decay of the peaks which define the local hexagonal order, i.e. the in-plane correlation peaks at $Q_1 = 0.039$ A^{-1} in the sector $\alpha = \pm 30°$, $\pm 90°$ and $\pm 150°$ and the peaks at $Q_3 = 0.028$ A^{-1} at $\alpha = \pm 90°$ corresponding to inter-plane correlations. In the final relaxation state the intensities show a Q^{-1} dependence at low Q which is a characteristic feature of short segments of dipolar chains. This shows that the hexagonal order gradually transforms to chain segments. Since the decay of the peak intensities was observed as well in the sum as in the difference patterns we conclude that nuclear inter-particle correlations disappear simultaneously with the magnetic correlations. The difference intensities averaged over boxes in the angle sectors at $\alpha = 90°$ and 30° are plotted in figure 14 as a function of time. All curves are well fitted by a single exponential decay according to

$$I(t) = y_0 + A\mathrm{e}^{-(t/\tau)} \tag{9}$$

where τ represents a characteristic relaxation time. While in the 30° sector the relaxation time $\tau(Q_1) = 3.4$ s is maximum at the in-plane correlation peak, $\tau(Q_3) = 2.4$ s, at the inter-plane correlation is considerably shorter. A continuous increase of τ was found in the vertical sector where the longest relaxation times of 6 s were found at $Q = 0.01$ A^{-1} which corresponds to the longest segments of chain composed by about 4–5 particles.

The rotation of the core–shell particle of volume V_p in a medium of viscosity η with a fixed dipole moment leads to a characteristic time τ_B for Brownian rotational diffusion given by

$$\tau_\mathrm{B} = 3\eta V_\mathrm{p}/k_\mathrm{B}T. \tag{10}$$

For free rotation of the magnetic dipole moment inside a fixed particle (Néel rotation) the characteristic time τ_N depends on the ratio between an activation energy E_A and the thermal energy. In the simplest case $E_\mathrm{A} = KV_\mathrm{c}$ where K is the shape anisotropy constant and V_c the core volume and τ_N is given by

$$\tau_\mathrm{N} = 1/f_0 \exp[KV_\mathrm{c}/k_\mathrm{B}T], \tag{11}$$

where f_0 is of the order of 10^9 Hz. Both mechanisms can occur simultaneously which should then lead to an apparent characteristic time $1/\tau_\mathrm{app} = 1/\tau_\mathrm{B} + 1/\tau_\mathrm{B}$. Using the structural parameters of the sample MFT3 [35] and $K = 2.6 \times 10^5$ J m^{-3} for fcc Co, $R_\mathrm{c} = (4.4 \pm 0.4)$ nm Néel relaxation times are expected in the range between 0.01 and 2600 s, i.e. at room temperature the majority of the moments must be blocked inside the particles. On the other hand for a single core–shell particle of radius $R_\mathrm{p} = (R_\mathrm{c} + D) = 6.4$–$9.5$ nm and the viscosity $\eta = 0.2$ Pa s for L9, the Brownian relaxation time τ_B ranges between 0.16 and 0.5 ms, which is by four orders of magnitude faster than observed. Reversely, Brownian relaxation times of 1–5 s imply large aggregates of the order of 100–200 nm which effectively correspond to the size of the locally ordered domains as derived from the widths of the structure factor peaks. In that picture the observed long relaxation times implies result from Brownian rotation of the whole ordered domain as the fastest process. The sticking of the particles inside the aggregates

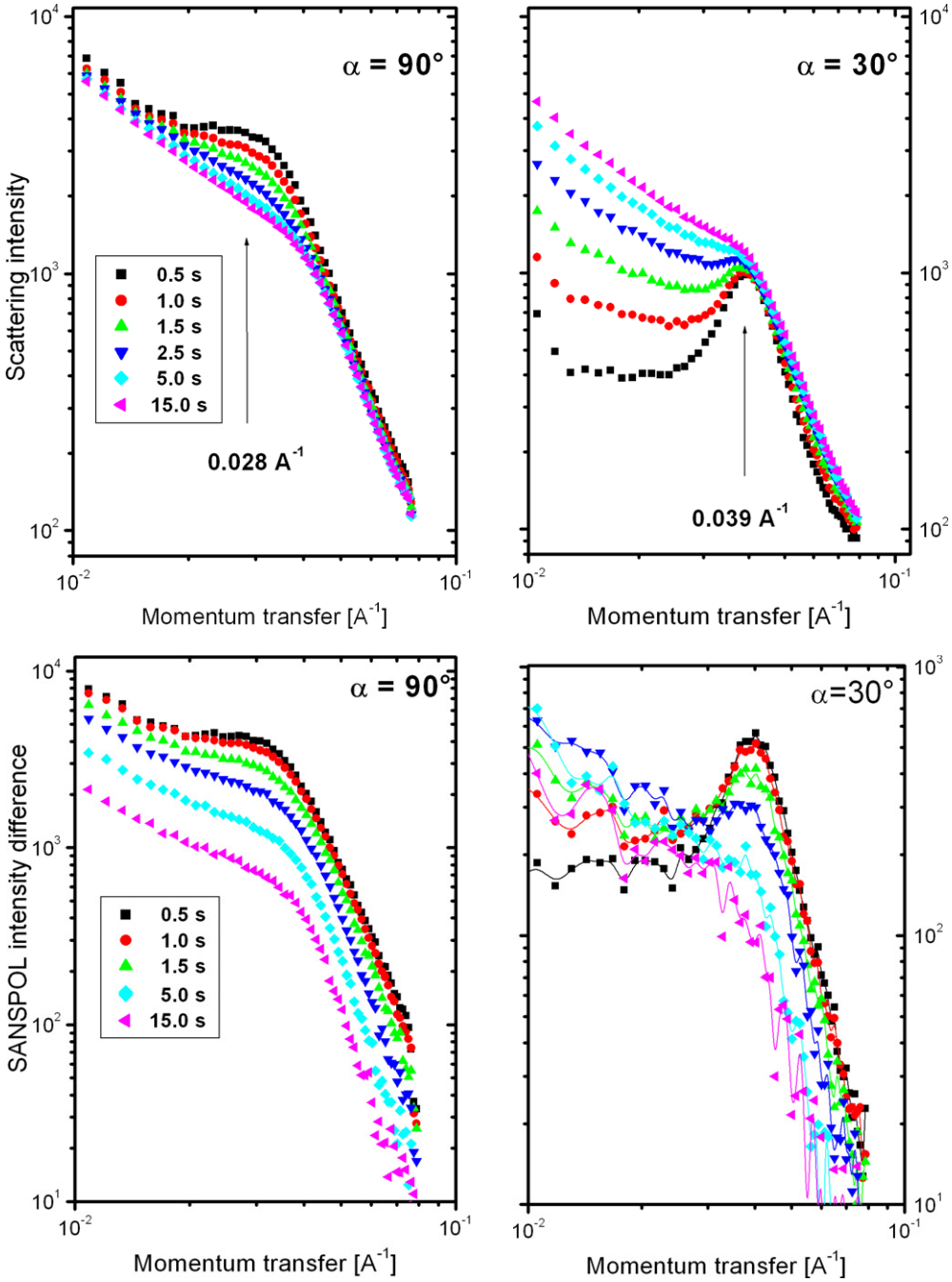

Figure 13. SANSPOL intensity sum $(I(+) + I(-))/2$ (upper row) and differences $I(+) - I(-)$ (lower row) in sectors $\alpha = 90°$ (lhs) and $\alpha = 30°$ (rhs) averaged over $\Delta\alpha = 20°$ at $t = 0.5$, 1, 1.5, 2.5, 5 and 15 s after switching off the magnetic field of $H = 0.5$ T.

which prevents the Brownian rotation of individual particles must be determined by the dipolar interaction of the magnetic moments induced by the strong external magnetic field. Since

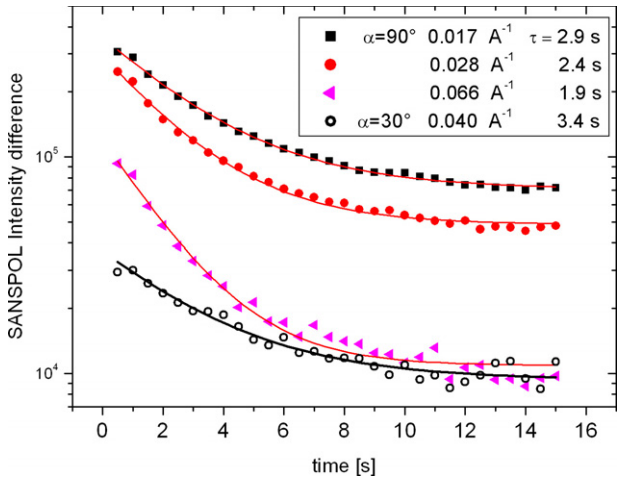

Figure 14. Time decay of the SANSPOL intensity differences in sectors perpendicular to H ($\alpha = 90°$) at different values of Q (solid symbols) and at Q_1 in the sector 30°. The solid lines correspond to fits of an exponential decay with the time constants τ which depend on Q.

dipolar interaction energy, given by

$$E_{dd} = (\mu o/4\pi) M_{\mathrm{sat}}^2 V_{\mathrm{c}}^2/\sigma^3, \tag{12}$$

depends on the distance σ and orientation of the particles in the ordered regions, the observed longer relaxation time for the intra-chain correlations could be due to the higher attractive dipole energy where $E_{dd}/k = 920$ K for a pair in closest contact $\sigma = 2(R_{\mathrm{c}}+2)$ is expected. For in-plane correlations at the mean distance of $a_h = 18.9$ nm $E_{dd}/kT = 300$ K and for the inter-plane interactions at $c_h = 21.9$ $E_{dd}/k = 190$ K are expected. Additional attractive interactions have been postulated in [40] to result from fluctuating parallel dipolar chains aligned along the field, slowing down the relaxation. Recent computer simulations give hints that in this concentrated colloid additional attractive sticking interactions occur between magnetic and non-magnetic micelles and surfactants which partly prevents particle rotation [41].

4.4. Discussion

The pseudo-crystalline lamellar hexagonal particle arrangement has never been observed experimentally before in magnetic colloids, where hard core repulsion competes with Van der Waals attraction and magnetic dipole–dipole interaction. As predicted in [45], the latter should give rise to a spontaneous arrangement of particles in chains or rings with magnetic moments parallel to each other. In an external magnetic field these chains are expected to be aligned along the field direction that gives rise to anisotropic structure factors. Dipolar chains are expected when the relative strength of the magnetic interaction $\gamma = E_{dd}/k_{\mathrm{B}}T$ exceeds 1–2. This was the case for magnetosomes where magnetite particles of 22 nm radius, covered by a lipid membrane of 2 nm thickness, spontaneously form long chains which are fully aligned in an external magnetic field [43]. Three dimensional ordered structures have been observed experimentally up to now only in dipolar systems with μm sized particles [40, 46] while the particle arrangement in nanosized FF is still controversial where isotropic network structures [47] and anisotropic concentration fluctuations [48] have been reported. Isotropic liquid-like structure factors have been reported in γ-Fe_2O_3 citrate FF with some kind of a vitreous transition when at very high volume fractions the dipolar interaction parameter was

of the order of $\gamma = 0.4$ [49]. On the other hand, recent computer simulations and theoretical work on electric dipolar systems revealed long range ferroelectric orientational order without positional order where hexagonal and fcc and bct structures have been found [50]. Modelling of competing repulsive and attractive interactions by rescaled mean sphere approximation seems to favour the formation of chains or chain segments at least for small values of γ [51]. For the present case of Co ferrofluids, where the actual parameters of $\langle R_c \rangle = 3.6$–$5.4$ nm, $D = 2$ nm and $M_{sat} = 1450$ kA m^{-1} correspond to interaction constant γ ranging between 1.4 and 8 the number of particles per chain is estimated between 10 and 40 for 1 and 5 vol% respectively [52]. Such spontaneous chaining in zero field has recently been observed by high resolution cryogenic electron microscopy [53]. The Q^{-1} behaviour of the scattering intensity observed at low Q in the direction perpendicular to the magnetic field confirms in fact the predictions of Monte Carlo simulations [40], i.e. some particle moments are really arranged in the attractive head to tail conformation and aligned along the field. However, interactions between fluctuating parallel dipolar chains which are aligned in a magnetic field can lead to attractions perpendicular to the field direction. This lateral attraction could in fact give rise to the observed lamellar structures. Effectively, molecular dynamics studies performed by Hess [54, 55] have predicted anisotropic structure factors when dipolar interaction exceeds the excluded volume effect. Above a critical value of the magnetic dipole moment a transition from the uniaxial to a lamellar, symmetry-breaking ordering should occur with almost close-packed in-plane structures. The results presented here experimentally confirm the presumed transition from field induced chain-like to lamellar ordering.

The dynamic SANS studies confirmed the formation of domains where particles are locally arranged in hexagonal symmetry with the moment direction stuck to the direction of the inducing magnetic field. When the field is switched off the fastest process is the rotation of the whole aggregate. Chain segments have been found as the most stable aggregates with the longest relaxation times.

5. Summary

The combination of SANSPOL with conventional contrast variation using different isotope mixtures of the carrier liquid allowed magnetic and non-magnetic particles to be distinguished and density, composition and magnetization profiles to be determined precisely. The microstructure parameters have been evaluated in polydisperse multiphase systems where magnetic materials (Co, Fe, magnetite), stabilization mechanisms (electrostatic, monolayers and bilayers of surfactants) and carrier liquids (water, organic solvents) have been systematically varied. As a common feature three different components were identified in the magnetic liquids: magnetic composite particles, non-magnetic micelles of organic shell molecules and magnetic aggregates. In diluted ferrofluids which are stabilized by surfactants composite particles are well described by a magnetic core and an organic shell of constant thickness. The size of the core depends on material and preparation conditions while the thickness of the shell is characteristic for the surfactant materials and depends on the carrier liquid. In the Co and magnetite ferrofluids the shell was found to be of homogeneous density and almost impenetrable for the solvent. In FeC based ferrofluids the shell can be penetrated partly by the carrier liquid. In Co FF which have been prepared by new techniques including 'smooth oxidation' a thin non-magnetic layer of $D = 1.5$ nm of CoO has been identified around the Co core, by which the samples are protected from further oxidation. No shell structure was found in charge stabilized samples where solvent molecules are in touch with the magnetic core. The magnetic nanostructure in diluted samples consists of non-interacting ferromagnetic single domain particles. Small amounts of aggregates with lower densities and magnetizations

and a typical size of 2–4 times the core radius were identified. This indicates that screening is incomplete in some systems, leading to aggregates in which surfactant molecules are included. Depending on preparation conditions, non-magnetic contributions have been found which are ascribed to free organic surfactants or micelles. In concentrated Co FF above 1 vol% Co interparticle interactions are induced by an applied external magnetic field that gives rise to an unexpected pseudo-crystalline ordering of cobalt core–shell particles. Particles are arranged in hexagonal planes, with the magnetic moments parallel to the [110] direction. The in-plane nearest neighbour distance is almost independent of the concentration and temperatures whereas the distance between neighbour planes strongly varies from sample to sample. The ordering follows the direction of the applied field, i.e. the magnetic moments and the [110] directions are always aligned along the magnetic field. In addition, segments of uncorrelated chains where the particle moments are arranged in the attractive head to tail conformation and aligned along the magnetic field were found to be present and frozen in when the carrier liquid is solidified. The dynamics of the field induced ordering has been studied by stroboscopic SANS which confirmed the presence of large ordered domains. Individual particle moments are stuck by field induced dipolar interactions into local hexagonal ordering which relax by a slow rotation of the whole domain when the field is switched off.

Acknowledgments

We thank Dr M Buske and Dr Gansau from Berlin, Professor H Bönnemann and Dr N Matussewitch from MPI Mühlheim for sample preparations. Fruitful collaborations with Dr A Hoell from HMI, Professor S Odenbach and Dr L Pop from the University of Dresden, Dr R May and Dr Ch Dewhurst from ILL, Grenoble, P Boesecke from ESRF Grenoble, Professor A Philipse, Dr K Butter, Dr G J Vroege and Dr B Erné from the van't Hoff Institute of Utrecht are gratefully acknowledged. This project was supported by the German research foundation (DFG) project No Wi 1151/2.

References

[1] Odenbach S (ed) 2002 *Ferrofluids—Magnetically Controllable Fluids and Their Applications* (*Lecture Notes in Physics* vol 594) (Berlin: Springer)
[2] 2005 *Proc. 10 Int. Conf. on Magnetic Fluids (Sao Paolo, 2004)*; *J. Magn. Magn. Mater.* **289**
[3] 2005 *Proc. 6th PAMIR Int. Conf. Fundamental and Applied MHD (Riga, 2005)*
[4] Wiedenmann A 1997 *J. Appl. Crystallogr.* **30** 580–5
[5] Kostorz G 1979 *Treatise on Materials Science and Technology* ed G Kostorz (New York: Academic) pp 227–90
[6] Percus J K and Yevick G J 1959 *Phys. Rev.* **110** 1–13
[7] Pedersen J S 1994 *J. Appl. Crystallogr.* **27** 595–608
[8] Moon R M, Riste T and Koehler W C 1969 *Phys. Rev.* **181** 920–31
[9] Pynn R, Hayter J B and Charles S W 1983 *Phys. Rev. Lett.* **51** 710
[10] Wiedenmann A 2001 *Physica* B **297** 226–33
[11] Wiedenmann A 2000 *J. Appl. Crystallogr.* **33** 428–32
[12] Kohlbrecher J, Wiedenmann A and Wollenberger H 1997 *Z. Phys.* **104** 1–4
[13] Kohlbrecher J 1996 *PhD Thesis* Technical University Berlin
[14] Wiedenmann A 2005 *Physica* B **356** 246–53
[15] Buske N, Sonntag H and Götze T 1984 *Colloids Surf.* **12** 195–202
[16] Khalafalla S E and Reimers G W 1980 *IEE Trans. Magn.* **16** 178–83
[17] Grünberg K, Wawer C, Tebo B M and Schüler D 2001 *Appl. Environ. Microbiol.* **67** 4573
[18] Butter K, Philipse A P and Vroege G J 2002 *J. Magn. Magn. Mater.* **252** 1–3
[19] Papirer E, Horny P, Balard H, Anthore R, Petipas C and Martinet A 1983 *J. Colloid Interface Sci.* **94** 207–19
[20] Hess P H and Parker P H 1933 *J. Appl. Polym. Sci.* **10** 1915–27
[21] Bönnemann H *et al* 2003 *Inorg. Chim. Acta* **350** 617–24

[22] Hasegawa M, Maruno S, Kawaguchi T and Moriya T 1992 *Proc. 6th Int. Conf. on Ferrite* S1007–10
[23] Keiderling U and Wiedenmann A 1995 *Physica* B **213/214** 895–7
[24] Keller T, Krist T, Danzig A, Keiderling U, Mezei F and Wiedenmann A 2000 *J. Nucl. Instrum.* A **451** 474–9
[25] Keiderling U 1997 *Physica* B **234–236** S1111–3
[26] Heinemann A and Wiedenmann A 2003 *J. Appl. Crystallogr.* **36** 845
[27] Wiedenmann A 2002 *Lecture Notes in Physics* vol 594 (Berlin: Springer) pp 33–58
[28] Heinemann A, Wiedenmann A, Kammel M, Bönnemann H and Matoussevitch N 2004 *Appl. Organometal. Chem.* **18** 561–4
[29] Kammel M, Wiedenmann A, Heinemann A, Bönnemann H and Matoussevitch N 2006 *Physica* B at press
[30] Butter K, Wiedenmann A, Hoell A, Petukhov A and Vroege G J 2004 *J. Appl. Crystallogr.* **37** 847–56
[31] Kammel M, Hoell A and Wiedenmann A 2001 *Scr. Mater.* **44** 2341–5
[32] Kammel M, Wiedenmann A and Hoell A 2002 *J. Magn. Magn. Mater.* **252** 89–91
[33] Hoell A, Kammel M, Heinemann A and Wiedenmann A 2003 *J. Appl. Crystallogr.* **36** 558–61
[34] Wiedenmann A, Hoell A, Kammel M and Boesecke P 2003 *Phys. Rev.* E **68** 031203
[35] Wiedenmann A and Heinemann A 2005 *J. Magn. Magn. Mater.* **289** 58–61
[36] Pop L M, Odenbach S, Wiedenmann A and Bönnemann H 2005 *J. Magn. Magn. Mater.* **289** 303–6
[37] Keiderling U, Wiedenmann A and Haug J 2006 *Physica* B at press
[38] Wiedenmann A, Keiderling U, May R P and Dewhurst C 2006 *Physica* B at press
[39] Wiedenmann A and Keiderling U 2006 at press
[40] Liu J, Lawrence E, Wu A, Ivey M, Flores G, Javier K, Bibette J and Richards J 1995 *Phys. Rev. Lett.* **74** 2828–3831
[41] Ilg P, private communication
[42] Heinemann A and Wiedenmann A 2005 *J. Magn. Magn. Mater.* **289** 149–51
[43] Hoell A, Wiedenmann A, Heyen U and Schüler D 2004 *Physica* B **350** e309–13
[44] Heinemann A, Hoell A, Wiedenmann A and Pop L P 2006 *Physica* B at press
[45] de Gennes P G and Pincus P A 1970 *Phys. Condens. Mater.* **11** 189
[46] Skjeltorp A T 1985 *J. Appl. Phys.* **57** 3285–90
[47] Camp Ph J and Patey G N 2000 *Rev.* E **62** 5403–8
[48] Hess S, Hayter J B and Pynn R 1984 *Mol. Phys.* **53** 1527
[49] Gazeau F, Dubois E, Bacri J-C, Boué F, Cebers A and Perzynski R 2002 *Phys. Rev.* E **65**
[50] Groh B and Dietrich S 2001 *Phys. Rev.* E **63** 021203
[51] Hayter J B 1988 *J. Appl. Crystallogr.* **21** 737–42
[52] Zubarev A Y 2001 *Colloid J.* **6** 338
[53] Butter K, Bomans P, Frederik P, Vroege G and Philipse A 2003 *Nat. Mater.* **252** 88
[54] Hess S 1987 *Physics of Complex and Supermolecular Fluids* ed S A Safran and N A Clark (New York: Wiley–Interscience) pp 631–42
[55] Hess S, Weider M and Kröger M 2001 *Magnetohydrodynamics* **37** 287